Journal of Nuclear Materials 392 (2009) 476–481

Contents lists available at ScienceDirect

Journal of Nuclear Materials

journal homepage: www.elsevier.com/locate/jnucmat

Evaluation of the depth-dependent yield strength of a nanoindented ion-irradiated Fe–Cr model alloy by using a finite element modeling

Chansun Shin [a,*], Hyung-ha Jin [a], Maan-Won Kim [b]

[a] Nuclear Materials Research Division, Korea Atomic Energy Research Institute, Daejeon 305-353, Republic of Korea
[b] GNEC Inc., 706 Toplip, Yuseong, Daejeon 305-510, Republic of Korea

ARTICLE INFO

Article history:
Received 9 October 2008
Accepted 13 April 2009

ABSTRACT

Ion bombardment of materials produces a shallow damaged region, in which the density of the radiation-induced defects is highly heterogeneous in depth from the irradiated surface. A nanoindentation on the surface of an ion-irradiated specimen probes the load-depth (L–h) response of the damaged region, which has varying mechanical property along the indentation depth. The measured nano-hardness thus is an average value of a varying hardness over the damaged region. The dose dependence of the increase in yield strength of an ion-irradiated Fe–Cr model alloy was evaluated by combining a nanoindentation test with a finite element (FE) modeling. The radiation damaged region was discretized into a finite number of layers with a pre-defined depth profile of the yield strength in terms of the dose level in the FE modeling. The dose-dependent yield strength and the intrinsic hardness of the damaged regions were extracted by comparing the computed L–h curve with the experimentally measured one.

1. Introduction

Irradiation experiments of materials by using high-energetic ions have been adopted as simulated experiments of a neutron irradiation to understand the radiation effects on the microstructures and mechanical properties in various nuclear materials [1–4]. The advantages of an ion-irradiation are a high damage rate which enables an investigation of the high dose effects and a negligibly induced radioactivity which makes a microstructural examination easy. Care must be taken, however, to predict the radiation damages at low damage rate experienced in commercial reactors since the correlation of the effects of a high and a low damage rate is not currently available. Thus, researches have been performed to investigate the role of a chemical composition, temperature, dose and radiation-damage mechanism qualitatively rather than to simulate the commercial reactor conditions directly.

Unlike electrons or neutrons, ions can penetrate to only a few micrometers from the surface of a specimen. As a result, an ion irradiated region extends only a few micrometers from the surface of a specimen and the irradiation damage level shows a depth-dependent profile. Indentation with a low load indenter (nanoindentation) is often applied to measure the changes in the mechanical properties of an ion-irradiated region. Nanoindentation is a depth-sensing indentation, and load is measured with respect to the penetration depth of an indenter. Mechanical properties, such as the hardness, Young's modulus can be extracted from the measured load–depth (L–h) curves [5].

Although a nanoindentation is widely used for a characterization of mechanical properties especially in small volumes, interpretation of the nanoindentation data of ion-irradiated specimens is still difficult because of the characteristic of an ion irradiated region: indentation probes a radiation-hardened region located on a soft, unirradiated matrix and the irradiated region has a depth changing mechanical property. Thus a special care is required to quantify the changes in the mechanical properties after an ion irradiation. To probe the hardness of a damaged layer, the load is controlled such that the indentation depth and plastic zone below an indenter contacts the damaged layer [1]. To measure the depth dependent hardness, a successive loading-unloading during indentation has been adopted [4], and an indentation with a continuous stiffness measurement (CSM) method has been applied [6].

To correlate the measured nano-hardness change with the yield strength change, Rice and Roger [7] showed that there are linear correlations between a nano-hardness and a Vickers hardness, and between a Vickers hardness and a yield strength in the case of ferritic alloys. A numerical method also exists to extract the elasto-plastic properties from measured L–h curves of a nanoindentation by using a FE modeling [8].

This article presents an attempt to extract the intrinsic mechanical properties of ion-irradiated specimens by combining a nanoindentation test with a FE modeling. We used an iron binary model alloy containing 9 wt% chromium irradiated by iron ions at room temperature. The interest in Fe–Cr model alloys is that these alloys

* Corresponding author. Tel.: +82 42 868 4953; fax: +82 42 868 5952.
E-mail address: cshin@kaeri.re.kr (C. Shin).

0022-3115/$ - see front matter © 2009 Elsevier B.V. All rights reserved.
doi:10.1016/j.jnucmat.2009.04.011

have a good resistance to a swelling, helium embrittlement and an irradiation creep [9,10]. Nanoindentation with a CSM technique was used to measure the L–h curves. The CSM technique allows for a continuous measurement of the hardness along the indentation depth [11]. We modeled the nanoindentation test by using a FE method, and the radiation damaged region was divided into a finite number of layers with a pre-defined depth profile of the yield strength in terms of the dose level in the FE modeling. We were able to evaluate the dose-dependent yield strength of the irradiated layers and estimate the intrinsic hardness of the maximum damaged layer. In the following, we first present the methodology for the sample preparation and the nanoindentation modeling. Then the results of the extracted mechanical properties of the unirradiated and irradiated specimens by using a FE modeling are discussed.

2. Methodology

2.1. Specimens and ion-irradiation conditions

Fe–9Cr (mass percent) model alloys were produced by melting electrolytic iron and chromium in a vacuum by an induction heating. A lump of the model alloy was then rolled into a 1 mm-thickness plate, and specimens were machined from the plate. The specimens were fully recrystallized at a temperature of 600–700 °C, and the final Vickers hardness was around 1 GPa.

Polygonal ferritic grains of the specimens were 10–50 μm in size, and two types of precipitates were observed: small precipitates with a size of ~50 nm and large inclusions with a size larger than 1 μm. Small precipitates are believed to be $Cr_{23}C_6$.

The Fe–9Cr alloy specimens were irradiated by using a 1.7 MeV Tandem VDG accelerator at Korea Institute of Geoscience and Mineral Resources (KIGAM), which can be operated in various conditions in terms of the dose, flux and specimen temperatures. The surfaces of the specimens were electro-chemically polished and then the specimens were irradiated by Fe^{4+} ions with acceleration energy of 2 MeV. The beam flux was 2.5×10^{11}–9.1×10^{11} ions/cm^2/s, and the dose was set to be 5.6×10^{14} ions/cm^2. The specimen was mounted on an aluminum sample holder using silver paste. The backside of the sample holder was air cooled to prevent excessive heating of the specimen during ion-irradiation. The temperature was monitored with a thermocouple on the sample holder close to the specimen. The measured temperature was found to stay less than 40 °C.

Fig. 1(a) shows a cross-sectional TEM micrograph of the ion-irradiated Fe–9Cr alloy. Small black dots represent radiation-induced defects, and the maximum damaged zone was observed at a depth of around 1.6 μm. Fig. 1(b) shows the calculated depth-dose profile of the Fe–9Cr alloy by using the SRIM code [12]. The calculated peak damage was ~1.1 dpa at a depth of around 1.75 μm from the surface, which is consistent with the TEM observation.

2.2. Nanoindentation tests

Nanoindentation was performed using a Nanoindenter XP system (MTS Nano Instruments) with a Berkovich type indenter normal to the unirradiated and irradiated Fe–9Cr specimens. The L–h curves were monitored in a displacement-controlled mode at a constant displacement rate, 3.8 nm/s. A total of nine indentations were made for each specimen. The spacing between the indentations was approximately 50 μm apart in order to avoid any overlap of a deformation region below each indentation. The depth profiles of the hardness were measured by using the CSM technique.

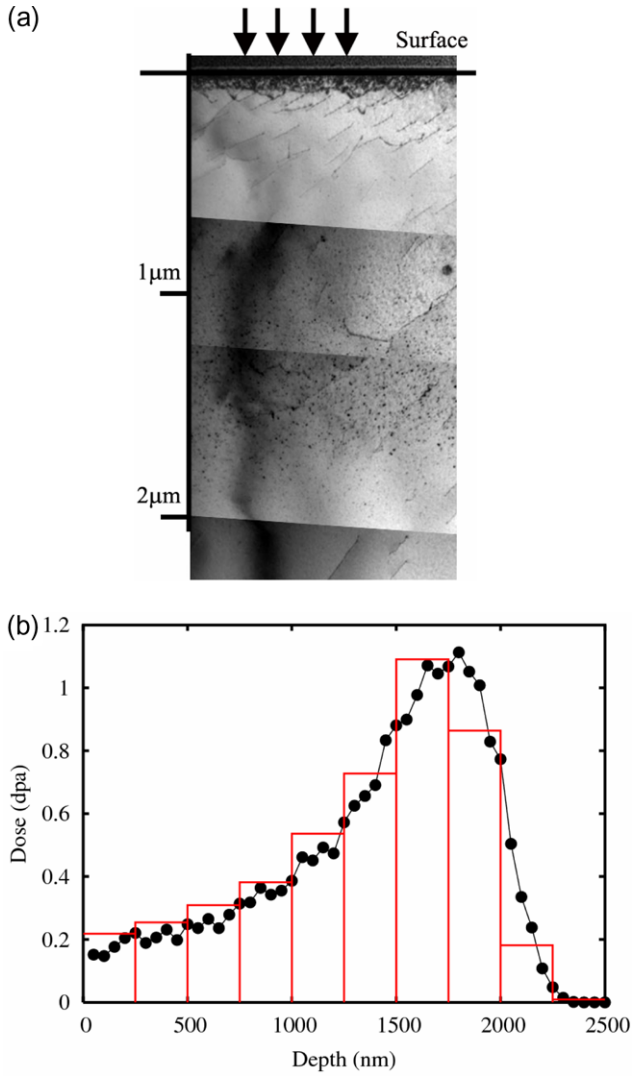

Fig. 1. (a) Cross-sectional TEM micrograph of ion-irradiated Fe–9Cr sample. Arrows indicate the direction of ion beams. (b) Depth profile of dose calculated by using the SRIM code. The histogram represents a simplified damage profile used in the FE modeling.

2.3. Finite element modeling

The nanoindentations were modeled as a two-dimensional axisymmetric model by using the commercial finite element program, ABAQUS (Hibbitt, Karlsson & Sorensen Inc.). A Berkovich indenter was modeled as a conical indenter. The area–height (A–h) function of the conical indenter is $A = \pi h^2 \tan^2 \theta$. In order to have the same A–h function as a Berkovich indenter whose A–h function is $A = 24.56h^2$, the apex angle of the conical indenter, θ, was chosen as 70.3°. Dao et al. [8] have shown that the computed L–h curves by using a conical indenter and a Berkovich indenter were identical.

The indenter was modeled as a rigid body by using a 2D analytic rigid shell with a tip radius to represent a blunting of the indenter, which is invariably present near a tip in real experiments. We found that the computed L–h curves of the nanoindentation were considerably affected by the tip radius of the indenter. Fig. 2(a) shows the effect of the tip radius on the L–h curve of fused silica, which is often used as a standard sample due to its isotropic material properties with the Young's modulus, $E = 73$ GPa, the yield strength, $\sigma_y = 710$ MPa and with no work hardening. Larger tip

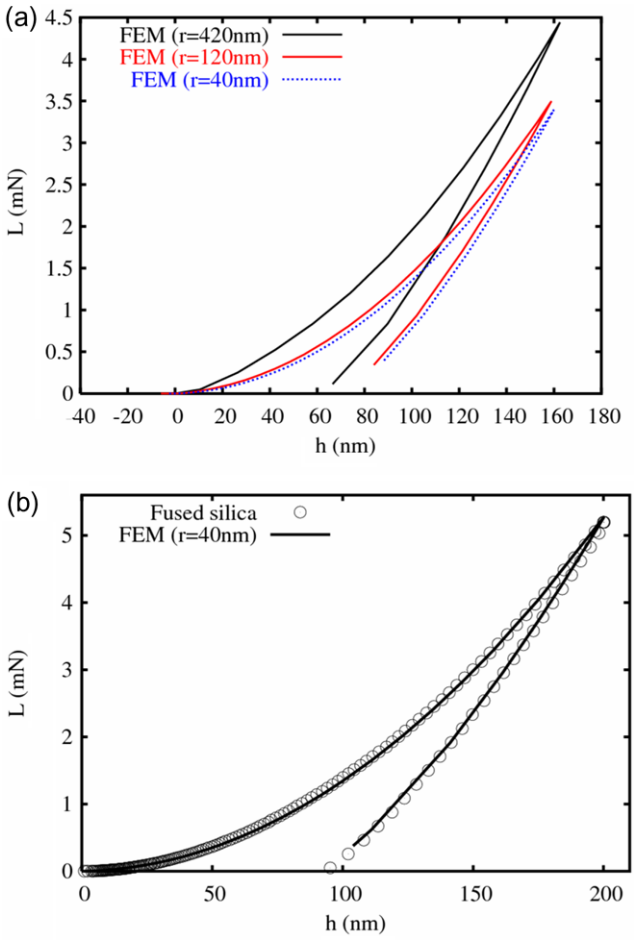

Fig. 2. (a) The effect of the tip radius of the conical indenter on the L–h curve for fused silica. (b) Comparison of the experimentally measured (circles) and the computed L–h curve (line) with the tip radius of 40 nm for fused silica.

radius shows a higher load at the same indentation depth. This is consistent with the Herzian elastic contact solution [13], which shows that the indentation load is proportional to the square root of the tip radius in the elastic loading regime. We found that the tip radius used in this study was 40 nm by comparing the modeled L–h curve with the calibration indentations of the fused silica as shown in Fig. 2(b).

Fig. 3 shows a typical FEM mesh used for a nano-indentation modeling. In order to represent a high stress and strain gradient well, the element size decreases near the point of contact with the indenter. The size of a specimen was 15 μm × 15 μm, and the size of an element just under the indenter was 5 nm × 10 nm.

A Fe–9Cr specimen was modeled as being locally isotropic, and the plastic flow of a specimen was governed by a uniaxial stress–strain curve through using the Mises yield criterion. The uniaxial stress–strain curve was represented by three parameters; the Young's modulus, E, the yield strength, σ_y, and the strain hardening coefficient, n, i.e. $\sigma = \sigma_y(1 + E/\sigma_y \cdot \varepsilon_p)^n$ after yielding, where ε_p represents a plastic strain.

A vertical displacement was prescribed on the indenter and the load response of a specimen was monitored by using a nonlinear static analysis. We used a contact friction value of 0.1 for the interaction between the indenter tip and the top surface of a specimen. It was shown that a friction coefficient varying from 0 to 1.0 had a negligible effect on the results [14].

In the following, the error for the simulated loads was measured as follows by using a mean squared error of a simulated load, L_s, to

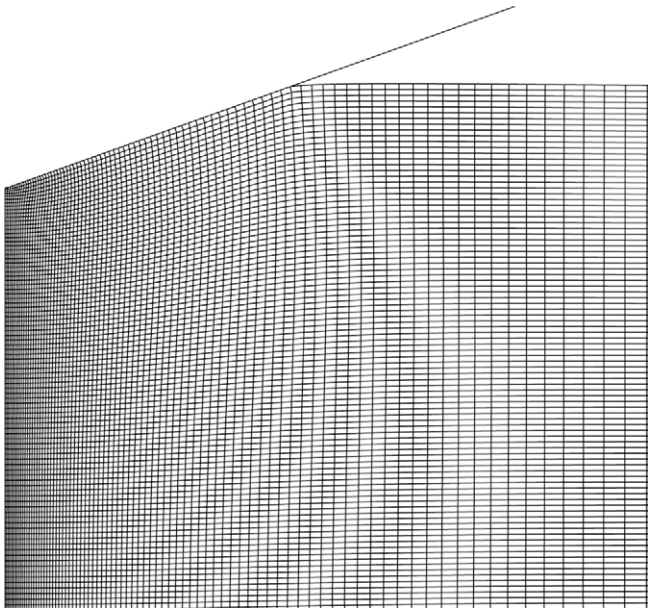

Fig. 3. Typical finite-element mesh used in the FE modeling of nanoindentation.

an experimentally measured load, L_m, at a specific indentation depth:

$$\text{Estimated error} = \frac{1}{N}\sum_{i=1}^{N}(L_s(h_i) - L_m(h_i))^2. \quad (1)$$

3. Results

3.1. Nanoindentation on unirradiated and irradiated Fe–9Cr

Fig. 4(a) shows the loading and unloading curves of the unirradiated (open circles) and irradiated (filled circles) Fe–9Cr specimens with an indentation depth up to 500 nm. The L–h curve during the loading stage of the indentation follows a typical relationship, $L = Kh^2$ for both cases. The load for the irradiated specimen rises much faster than that for the unirradiated specimen with the indentation depth. The initial slopes of both the unloading curves were found to be almost identical, which the means that unirradiated and irradiated specimens have the same reduced elastic modulus [5].

Depth profiles of the hardness measured by using the CSM method are shown in Fig. 4(b). Error bars represent the standard deviation in the measured values. The hardness data showed a large fluctuation at an indentation depth below 70 nm. This is presumably due to the surface roughness of the specimens. Thus the data with the indentation depth lower than 70 nm were omitted in Fig. 4(b). The hardness of the irradiated specimen (filled circles) showed a variation with the indentation depth, whereas the unirradiated specimen had an almost constant hardness of 1.6 GPa irrespective of the indentation depth. The maximum hardness of the irradiated specimen was measured at a depth of 250–300 nm; thus the indentation depth of the maximum hardness is around six times smaller that the depth of the maximum damaged location (Fig. 1(b)). This is because the maximum hardness occurs when the deformation region below the indenter reaches the maximum damaged layer, where moving dislocations are blocked by the radiation-induced defects [6].

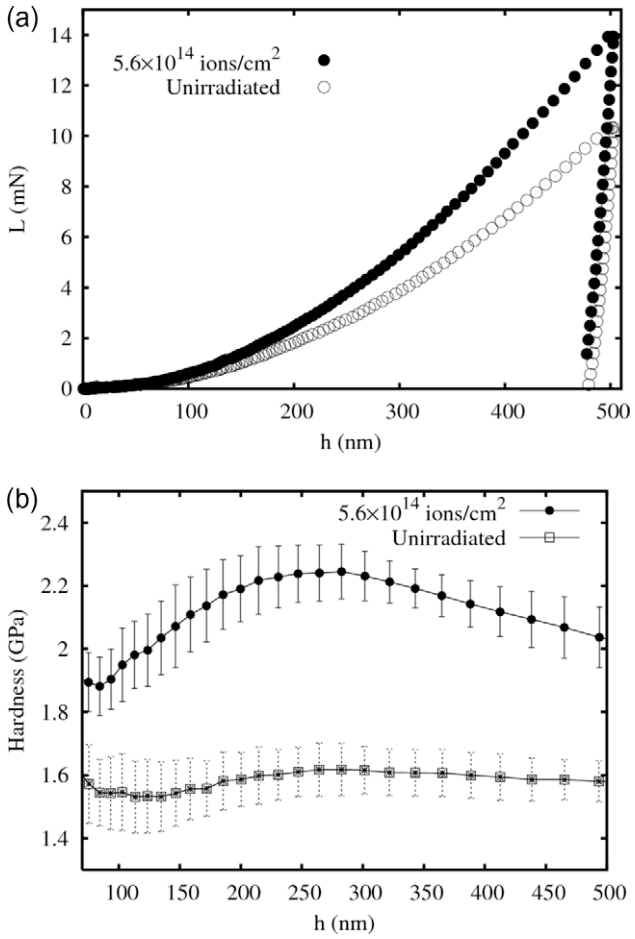

Fig. 4. (a) Measured L–h curves for irradiated (filled circles) and unirradiated (open circles) Fe–9Cr. (b) Depth profile of nano-hardness for irradiated (filled circles) and unirradiated (open squares) Fe–9Cr.

3.2. FEM modeling of an unirradiated specimen

The parameters of the uniaxial stress–strain curve for the unirradiated Fe–9Cr specimen were evaluated by comparing the experimentally observed L–h curves with the computed curves. We limited the unknown parameters to E and σ_y. n was determined to be 0.29 from a separate uniaxial tensile test. Two unknown parameters (E, σ_y) were searched by the following procedure; (i) by assuming a trial set of E and σ_y, a L–h curve was computed by using the FEM modeling presented in Section 2.3, (ii) the load at a depth of 465 nm and the stiffness of an unloading curve were compared to the experimentally measured values, (iii) a new trial set of E and σ_y was generated and a new L–h curve computed with a new trial set was tested. We generated a new trial set by noting that an increasing E increases the stiffness and an increasing σ_y increases the load at a specific depth.

Fig. 5 demonstrates the trial sets of E and σ_y, and the comparison between the computed and the experimentally measured load and stiffness data. The parameter set of $E = 164$ GPa and $\sigma_y = 265$ MPa was found to show a good match to the experimental data.

Simulated L–h curve by using the parameter set of $E = 164$ GPa and $\sigma_y = 265$ MPa is shown by a dashed line in Fig. 6(a) along with the experimental data. Fig. 6(b) demonstrates the difference between L_s and L_m, $\Delta L = L_s - L_m$. Fig. 6(b) shows that L_s underestimates L_m data below a depth of 400 nm and it overestimates the load above 400 nm. The underestimation of a loading curve at a shallow indentation depth was also reported by Myers et al. [15]. The authors suggested that an increased load in the near-surface region may result from a delayed plasticity in well annealed grains. Note that the Fe–9Cr specimens were fully recrystallized and the

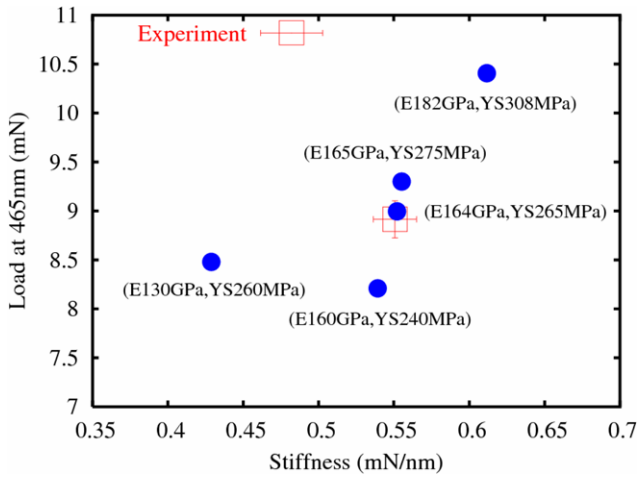

Fig. 5. Load and stiffness values (filled circles) computed by using the trial parameters of E and σ_y in brackets and the experimentally measured load and stiffness data (open square) with error bars.

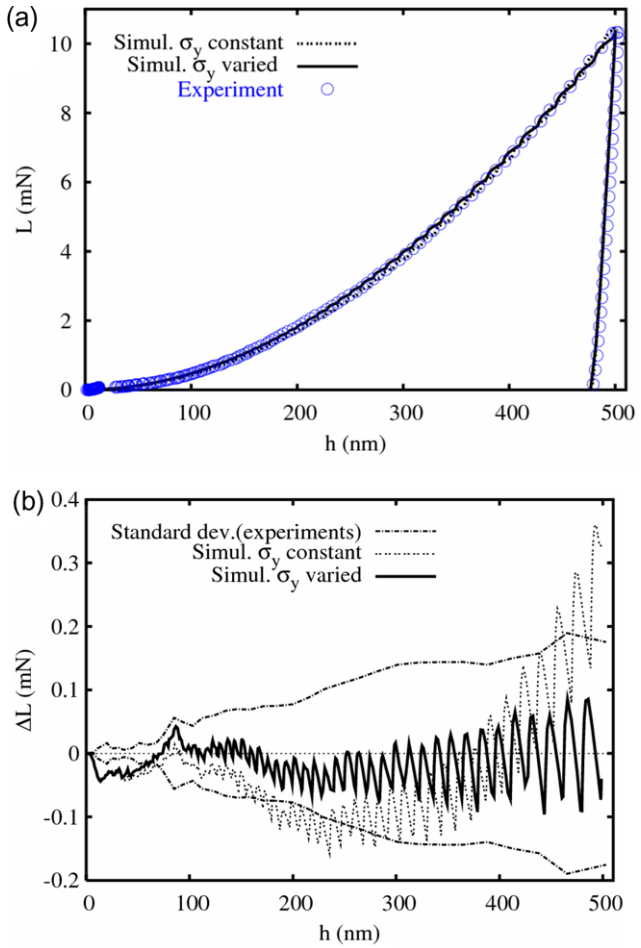

Fig. 6. (a) L–h curve (dashed line) simulated with the optimum parameters found in Fig. 5, and L–h curve (solid line) simulated with the depth profile of σ_y represented in Fig. 8 for unirradiated Fe–9Cr. (b) Difference between computed and measured loading curve for unirradiated Fe–9Cr.

surface was electrochemically polished. The deviation in the load could be reduced by increasing σ_y at a small depth. Increasing the near surface value of σ_y to 300 MPa was found to dramatically decrease the deviation from the experimental results. Solid line in Fig. 6(a) and (b) represents the simulation result by using the depth-dependent yield strength shown in Fig. 8, in which σ_y decreases from 300 MPa at a surface to 265 MPa at 2 μm depth. The error in L_s now comes within the standard deviation of the experimental data. The mean squared error of L_s (Eq. (1)) was decreased from 0.0115 to 0.0012 by using the depth-dependent yield strength. Note that L_s below a 70 nm indentation depth always showed a negative deviation compared to L_m. This is because the FEM modeling assumed that the material yields once the stress exceeds the Mises yield criterion, whereas experimentally the local stress can reach the theoretical strength of metals at a shallow indentation depth [16].

3.3. FEM modeling of an irradiated specimen

The irradiated specimen had a damaged zone whose damage level is depth-dependent. The radiation damaged zone was discretized into ten different layers as shown in Fig. 1(b). The relative height of each column in Fig. 1(b) was set to be a relative damage level. Mechanical properties of each different layer were assumed as follows; (i) E was assumed as invariable with the damage level, (ii) n was assumed to be constant, (iii) an increase in $\sigma_y(\Delta\sigma_y)$ was assumed to be proportional to a power of the relative damage level. The unaffected region with a depth larger than 2.25 μm retained the mechanical properties of unirradiated specimen as discussed in the previous section.

A constant E appears to be reasonable, since the unloading curve of both the unirradiated and irradiated specimens showed an identical slope (Fig. 4(a)). A numerous studies showed that $\Delta\sigma_y$ is increased with irradiation dose and saturated at higher doses at temperatures below 220 °C [17,18]. The dose-dependence of $\Delta\sigma_y$ is often expressed in the form of the power-law expression, $\Delta\sigma_y = A\Phi^p$, where Φ represents the radiation fluence [19]. Indeed, the dose-dependence of $\Delta\sigma_y$ of various metals was found to be characterized by using two power-law expressions for the low-dose and high-dose regime: the exponent p is much reduced for the high-dose regime [17]. The saturation hardening can be also expressed in the form of the exponential function, $\Delta\sigma_y = A[1 - \exp(-B\Phi)]^p$ [20]. The exponent p for low dose is estimated to be 0.5 from barrier hardening models [20]. However, a deviation from a value of 0.5 has been reported in some of pure metals [17,21]. Transition dose to saturation for bcc iron alloys is reported to be scattered: ~0.05 dpa for the neutron-irradiated case [17], and ~1 dpa for spallation proton-irradiated case [18].

We used the power-law expression without the saturation in this study for simplicity, although any form of the expression can be used in the FE modeling. We assumed that the yield strength increment for ith layer ($\Delta\sigma_y^i$) has a relation with the relative damage level (Φ^i as $\Delta\sigma_y^i = A(\Phi^i)^p$, where A is the yield strength increment of the maximum damaged layer. The exponent p is chosen either 0.5 or 0.25, because various steels having the initial σ_y larger than 440 MPa showed $p \sim 0.5$, whereas low alloyed irons having the initial σ_y lower than 220 MPa showed $p \sim 0.25$ for a low-dose regime [17].

Based on the damage profile in Fig. 1(b) and the relation for the $\Delta\sigma_y$ as given above, the unknown parameter, A, was searched for by performing numerous trial simulations. Fig. 7(a) shows the estimated error (Eq. (1)) of the computed L–h curve by changing A. We obtained an optimum value of A = 350 MPa for the $\Delta\sigma_y^i = A(\Phi^i)^{0.25}$ relation, and A = 450 MPa for the $\Delta\sigma_y^i = A(\Phi^i)^{0.5}$ relation. The overall computed L–h curves are compared to the experimental results in Fig. 7(b). The two relations for the $\Delta\sigma_y$ were found to simulate the loading behavior of the nanoindentation of the irradiated specimen well. The distributions of the $\Delta\sigma_y$ of each layer are presented in Fig. 8 for the two relations along with the depth-dependent yield strength distribution evaluated for the unirradiated specimen.

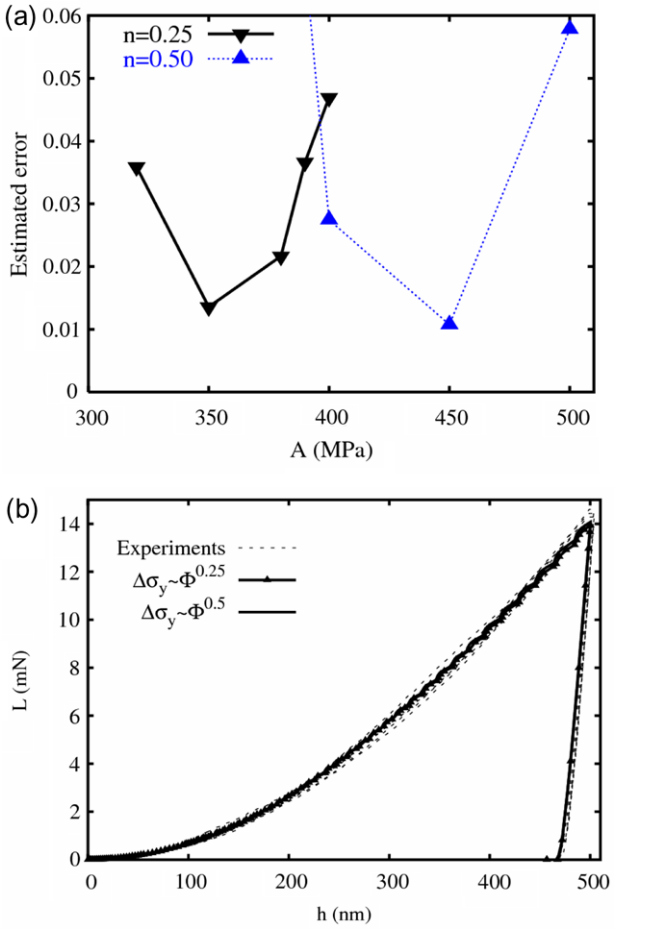

Fig. 7. (a) Estimated errors of the computed L–h curves using $\Delta\sigma_y^i = A(\Phi^i)^{0.25}$ (inverse triangles) and $\Delta\sigma_y^i = A(\Phi^i)^{0.5}$ relation (regular triangles). (b) Comparison between the measured L–h curves (dashed lines) and the simulated curves by using the $\Delta\sigma_y - \Phi$ relations.

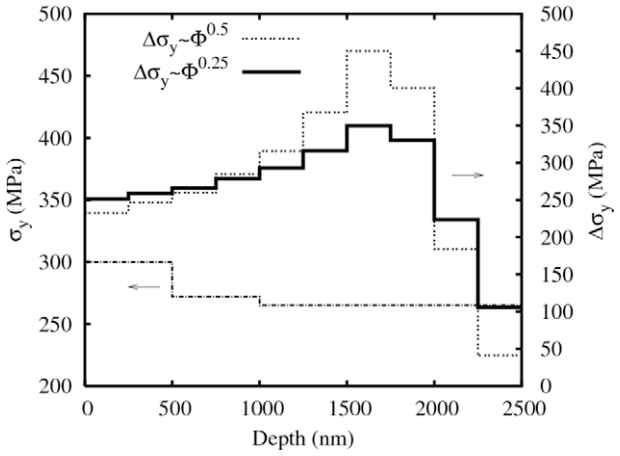

Fig. 8. Depth profile of σ_y for unirradiated Fe–9Cr (dash-dotted line) and depth profile of $\Delta\sigma_y$ for irradiated Fe–9Cr for each $\Delta\sigma_y - \Phi$ relation.

Table 1
The indentation load ratio at an indentation depth of 500 nm of the Fe–9Cr specimen irradiated up to 2.8×10^{15} ions/cm^2 to irradiated up to 5.6×10^{14} ions/cm^2.

	Experiments	$\Delta\sigma_y \sim \Phi^{0.25}$	$\Delta\sigma \sim \Phi^{0.5}$
Load ratio	1.08∼1.12	1.12	1.28

The validity of each $\Delta\sigma_y - \Phi$ relation for the Fe–9Cr alloy is evaluated in Section 4.

4. Discussion

The L–h curve of the irradiated Fe–9Cr alloy to a dose of 5.6×10^{14} ions/cm^2 was found to be well computed by using both the relation $\Delta\sigma_y^i = A(\Phi^i)^{0.25}$ with $A = 350$ MPa and $\Delta\sigma_y^i = A(\Phi^i)^{0.5}$ with $A = 450$ MPa. In order to verify which relation is more adequate for this material, we prepared another specimen irradiated to a five times higher dose, i.e. a dose of 2.8×10^{15} ions/cm^2. The ratio of the indentation load at an indentation depth of 500 nm of 2.8×10^{15} ions/cm^2 dose to that of 5.6×10^{14} ions/cm^2 dose was 1.08–1.12, i.e. higher dose induces higher hardening. The computed load ratio by using the relation $\Delta\sigma_y^i = A(\Phi^i)^{0.25}$ was 1.12, whereas the relation $\Delta\sigma_y^i = A(\Phi^i)^{0.5}$ resulted in a much higher ratio of 1.28 as listed in Table 1. Note that A values for each relation were retained and only Φ^i was multiplied by five for each layer. This result suggests that the expression, $\Delta\sigma_y = A\Phi^{0.5}$, cannot characterize the irradiated Fe–9Cr up to a dose of 2.8×10^{15} ions/cm^2, because the saturation probably sets in at a dose higher than 5.6×10^{14} ions/cm^2. $\Delta\sigma_y$ of the irradiated Fe–9Cr was found to be represented as the fourth root of a dose up to 2.8×10^{15} ions/cm^2 even without considering the saturation.

Correlation of the nano-hardness (NH) with the yield strength (YS) was investigated by Rice and Stoller [7]. The authors found that NH measured at a constant indentation depth of 400 nm correlates with a Vickers hardness (VH) measured using a 200-g load by the relation, NH = 1.06VH + 0.5, where the units are GPa for both NH and VH. Increasing the nanoindenation depth was found to decrease the intercept of the relation. YS is also proportional to VH with the relation, YS = 279(VH − 0.22), where YS is in MPa and VH in GPa.

The NH of the unirradiated Fe–9Cr was ∼1.6 GPa, and this value correlates to YS of 229 MPa by assuming that the NH–VH and VH–YS relations are still valid for the Fe–9Cr alloy. If we further assume that the intercepts of the NH–VH relation decrease to 0.4 for a nanoindenation with a depth of 500 nm, the YS of an unirradiated Fe–9Cr specimen is expected to be 254 MPa. Note that the estimated YS by using the NH–YS correlation agrees well with the computed YS, 265 MPa, by using the FE modeling.

The NH increased by ∼0.65 GPa due to the irradiation as shown in Fig. 4(b). $\Delta\sigma_y$ is estimated to be ∼170 MPa by using the correlations between NH, VH and YS. The estimated value is much lower than the computed $\Delta\sigma_y$ (Fig. 8). Note however that the measured NH is expected to be lower than the intrinsic hardness of an irradiate-hardened region, since the hardened layers are pushed into the much softer material which is unirradiated due to a limited penetration of the ions. We evaluated the intrinsic hardness of the maximum damaged layer, i.e. which has the maximum dose level in Fig. 1(b), by using the computed mechanical properties of the layer. We found that the hardness of the maximum damaged layer alone is ∼3 GPa, which is greater than the experimentally obtained value of 2.25 GPa as expected. The NH–VH relation results in an estimation value of $\Delta\sigma_y \sim 368$ MPa for the maximum damaged layer, which agrees well with the computed $\Delta\sigma_y$, 350 MPa.

5. Summary

In this work, we noted that the depth-dependent damage level affects the NH measured on the surface of ion-irradiated materials. The measured value is an averaged value of a changing hardness according to the depth profile of a damage level within an irradiated region. Thus the intrinsic hardness of the peak damaged region is expected to be higher than the measured value.

We applied a FE modeling in order to quantitatively evaluate the depth profile of yield strength and intrinsic hardness of ion-irradiated Fe–9Cr. The Young's modulus and the yield strength, which were used as unknown parameters in a FE modeling, could be evaluated in a few trial simulations by comparing with the experimentally measured L–h curves. We found that the computed yield strength of the unirradiated Fe–9Cr alloy agreed well with the estimated value from the measured NH. In the FE modeling of the ion-irradiated Fe–9Cr specimen, the ion-irradiated region was divided into a certain number of discrete layers, and $\Delta\sigma_y$ of each layer was expressed in the form of power-law expression, $\Delta\sigma_y - \Phi^p$. Our computation showed that $\Delta\sigma_y$ of the ion-irradiated Fe–9Cr can be represented with $p = 0.25$. $\Delta\sigma_y$ of the peak damaged layer was estimated to be ∼368 MPa from the computed intrinsic hardness, whereas $\Delta\sigma_y$ is estimated to be ∼170 MPa from the measured NH. This result clearly shows that the measured NH value leads to an underestimation of $\Delta\sigma_y$ for the peak damaged region.

In summary, this work showed that the yield strengths and intrinsic hardness of an ion-irradiated region which vary with depth can be evaluated by combining nanoindentation tests with a FE modeling as proposed in this study.

References

[1] M. Ando, Y. Katoh, H. Tanigawa, A. Kohyama, J. Nucl. Mater. 271&272 (1999) 111.
[2] K. Yasunaga, H. Watanabe, N. Yoshida, T. Muroga, N. Noda, J. Nucl. Mater. 283–287 (2000) 179.
[3] N. Sekimura, T. Kamada, Y. Wakasugi, T. Okita, Y. Arai, J. Nucl. Mater. 307–311 (2002) 308.
[4] Y. Katoh, M. Ando, A. Kohyama, J. Nucl. Mater. 323 (2003) 251.
[5] W.C. Oliver, G.M. Pharr, J. Mater. Res. 7 (1992) 1564.
[6] S. Taniguchi, A. Kitahara, S. Wakayama, E. Eriguchi, N. Suyama, Nucl. Instrum. and Meth. B 175–177 (2001) 647.
[7] P.M. Rice, R.E. Stoller, Mat. Res. Soc. Symp. Proc. 649 (2000) Q7.11.1.
[8] M. Dao, N. Chollacoop, K.J. Van Vliet, T.A. Venkatesh, S. Suresh, Acta Mater. 49 (2001) 3899.
[9] D.S. Gelles, J. Nucl. Mater. 225 (1995) 163.
[10] P.J. Karditsas, Fus. Eng. Des. 48 (2000) 527.
[11] X. Li, B. Bhushan, Mater. Charact. 48 (2002) 11.
[12] SRIM software packages, <http://www.srim.org>.
[13] H.L. Johnson, Contact Mechanics, Cambridge University, Cambridge, UK, 1985.
[14] J.A. Knapp, D.M. Follstaedt, S.M. Myers, J.C. barbour, T.A. Friedmann, J. Appl. Phys. 85 (1999) 1460.
[15] S.M. Myers, J.A. Knapp, D.M. Follstaedt, M.T. Dugger, J. Appl. Phys. 83 (1998) 1256.
[16] S. Shim, H. Bei, E.P. George, G.M. Pharr, Scripta Mater. 59 (2008) 1095.
[17] T.S. Byun, K. Farrell, J. Nucl. Mater. 326 (2004) 86.
[18] T. Yamamoto, G.R. Odette, H. Kishimoto, J.-W. Rensman, P. Miao, J. Nucl. Mater. 356 (2006) 27.
[19] T.H. Blewitt, R.R. Coltman, R.E. Jamison, J.K. Redman, J. Nucl. Mater. 2 (1960) 277.
[20] M.J. Makin, F.J. Minter, Acta Metall. 8 (1960) 691.
[21] S.J. Zinkle, J. Nucl. Mater. 150 (1987) 140.